Crystallization Kinetics of Amorphous NiTi Shape Memory Alloy Thin Films

Xi Wang, Joost J. Vlassak[*]

Division of Engineering and Applied Sciences, Harvard University, Cambridge, MA 02138, USA

Abstract

The temperature dependence of the crystallite nucleation and growth rates is measured for amorphous NiTi thin films. Using TEM, crystallites are shown to nucleate homogeneously in the film and to grow in a channeling mode. A mechanism that suppresses heterogeneous nucleation is proposed. By manipulating nucleation and growth rates, grains as large as 60 μm can be obtained in submicron films.

Keywords: Shape memory alloy thin films; Crystallization kinetics; Activation energy; Grain size

---

[*] Corresponding author. Tel.: +1 617 496 0424; fax: +1 617 495 9837. *E-mail address*: vlassak@esag.harvard.edu (J.J. Vlassak)

1. Introduction

Shape memory alloys (SMAs) are active materials that derive their unique properties from a thermoelastic martensitic transformation. They have been studied extensively over the last 50 years with most attention focused on bulk materials. Recently, it was shown that thin films of these alloys also exhibit shape memory properties [1,2,3,4,5,6,7], making them attractive candidates for use as actuators in microelectromechanical systems (MEMS). The transformation behavior of a shape memory alloy depends sensitively on its microstructure [8,9]. NiTi thin films sputter-deposited at room temperature are usually amorphous in their as-deposited state. This observation provides an opportunity to control the microstructure by adjusting the crystallization conditions. Therefore, it is important to understand crystallization kinetics of this material. The crystallization of NiTi has been characterized as polymorphic with continuous nucleation and growth throughout the crystallization process based on in-situ transmission electron microscopy studies [10,11]. To the best of our knowledge, systematic measurements of the crystal nucleation rate and growth velocity as a function of temperature have not been performed. From classic transformation theory, it is well known that those two quantities are essential to the definition of the final microstructure, in that they determine the grain size of the material. In the present study, we used a combined approach of annealing in a high-precision furnace and microscopic tracking of individual crystallites to determine the temperature dependence of the crystal nucleation rate and growth velocity in amorphous NiTi thin films. This approach was first developed by Kalb *et al.* for the study of thin films of amorphous Te alloys [12]. Due to the densification that takes place upon crystallization, the film thickness can be reduced by as much as 5% enabling direct observation of the crystallites using atomic force microscopy (AFM) or by optical microscopy as light scatters from the crystallite boundaries. Moreover, the surface relief caused by the

martensitic phase transformation inside crystalline particles is also readily observed using these techniques. Optical microscopy was used in this study predominantly because it provides much better statistics than AFM: AFM scan size is limited to 80x80 μm while crystals can be as large as 80 μm under certain conditions.

2. Experimental

Near-equiatomic NiTi thin films with a thickness of approximately 800 nm were deposited on LPCVD Si_3N_4 (thickness 80 nm) coated (100) silicon substrates by means of dc magnetron sputtering. The composition of the films was measured to be 50.5±0.2 at%Ti using Rutherford Backscattering Spectrometry (RBS). Immediately after deposition, the NiTi films were coated with approximately 30 nm of PECVD SiN_x to prevent excessive oxidation of the films. The NiTi samples were annealed isothermally in a furnace of a Perkin-Elmer Pyris 1 differential scanning calorimeter (DSC) in a flowing argon atmosphere. The samples were cut into small square pieces of 4x4 mm to fit into the DSC furnace (dimensions: 9 mm diameter x 4 mm height). The heating rate was 500 ^{o}C/min and there was no overshoot on approaching the final temperature. The temperature uncertainty during annealing was less than 0.1 ^{o}C. Samples were annealed isothermally at temperatures ranging from 410 ^{o}C to 445 ^{o}C. After annealing for a certain period of time, each sample was investigated under an optical microscope. The sample was then returned to the furnace and annealed at the same temperature for an additional period of time, followed by observation under the optical microscope at the exact same location. This annealing/observation process was repeated until each sample was fully crystallized. The isothermal crystal growth velocity was determined by measuring the increase in diameter of specific crystals from subsequent optical micrographs. The nucleation parameters were

determined based on the methodology developed by Kˆster and Blanke [13]. The time of nucleation for each crystal was back-extrapolated by measuring its size at the end of the heat treatment and using the growth kinetics determined earlier.

Plan-view TEM specimens were prepared by ultrasonically cutting 3 mm diameter discs from the samples. The discs were dimpled and the area of interest was thinned to electron transparency by ion beam milling. Cross-section TEM samples were prepared by mechanical tripod polishing and ion beam milling. Samples were examined in a JEOL 2010 FEG transmission electron microscope operated at 200 kV.

3. Results and discussion

3.1. Crystallization morphology by transmission electron microscopy

Fig. 1 is a cross-section TEM micrograph of a crystal in a partially crystallized film. The crystal is disk-shaped and is much longer laterally than in the through-thickness direction. A closer look at the image shows that the crystal has not yet reached the interface or surface of the film and that thin amorphous layers remain at these locations. This indicates that the crystal nucleates inside the film; heterogeneous nucleation at an interface was not observed. We explain the absence of heterogeneous nucleation in these films as a result of the dependence of the crystallization kinetics on the precise composition of the NiTi alloy. The crystallization temperature and the crystallization activation energy decrease with increasing Ti concentration and apparently reach a minimum near the composition of $NiTi_2$ [14,15]. Quantitative composition analysis of the residual amorphous layers in Fig. 1 shows that both amorphous layers are Ni-rich while the bulk of the film is near-equiatomic. The Ti depletion is caused by oxidation of NiTi prior to the deposition of the PECVD SiN_x or by reaction of NiTi with the underlying LPCVD SiN_x; a Ti-depleted region of a few nanometers seems to be sufficient to

suppress nucleation at the interfaces with the SiN_x coatings. Consequently, nucleation takes place homogenously inside the film and the crystals grow in a ìchannelingî growth mode. Eventually, the grains extend all the way to the interfaces. The morphology of the crystals clearly indicates that the nuclei quickly consume most of the film thickness, and then transition to a two-dimensional growth mode. This results in the disk-shaped grains observed in plan-view TEM micrographs (Fig. 2). Some crystals are nearly circular, while others show slight shape anisotropy. The shape anisotropy is due to a slight orientation dependence of the growth velocity and whether it can be observed depends on the orientation of the grain.

3.2 Kinetics of crystallization

Fig. 3 shows a series of optical micrographs for a sample annealed at 435 ^{o}C. While existing crystals are growing, new nuclei appear at random in the untransformed regions throughout the crystallization process. The isothermal growth velocity was determined by measuring the diameter of grains in subsequent optical micrographs. The isothermal crystal growth velocity was observed to be constant over the temperature range investigated, i.e., it is size and time-independent at a given temperature. This confirms that the growth process is interface-controlled, in agreement with the observation that there is no composition change across the growth front. Fig. 4 is an Arrhenius plot of the crystal growth velocities. The fitting parameters obtained from the Arrhenius fits are listed in Table 1.

Fig. 5 shows the number of nuclei as a function of time for crystallization at 445 ^{o}C. The results were obtained using the back-extrapolation procedure, the validity of which is supported by the TEM observations (see section 3.1). Each particle arises from one nucleation center, no multi-grain clusters are observed as in $Ti_{50}Ni_{25}Cu_{25}$ melt-spun ribbon [16]. The number of nuclei, $N(t)$, is shown normalized by the fraction of untransformed volume since crystals only nucleate

inside the amorphous regions of the films. The number of nuclei is initially extremely small, but increases linearly after an incubation period. The nucleation rate $I(t)$ is obtained from

$$I(t) = \frac{1}{1-\chi(t)} \frac{dN(t)}{dt},$$ (1)

where $\chi(t)$ is the crystallized fraction at time t. The time lag τ is defined as the initial transient period before the steady-state nucleation rate I_{ss} is reached. The Arrhenius graphs of the steady-state nucleation rate and the time lag are shown in Fig. 6; the corresponding Arrhenius parameters are listed in Table 1. According to classical nucleation theory [17], the activation energy E_n for the steady-sate nucleation process is given by

$$E_n = \Delta G_c + E_g,$$ (2)

where ΔG_c is the energy barrier for the formation of a critical nucleus and E_g is the activation energy for growth. Since TEM observations indicate that nucleation occurs homogeneously, the nucleation barrier for homogenous nucleation in near-equiatomic NiTi is estimated at 2.60±0.19 eV.

The activation energies obtained in this study are compared to literature data for both bulk NiTi [14,18,19] and for thin films [20] in Fig. 7. Most activation energies in the literature are measured using DSC and represent the activation energy for the overall crystallization process, i.e., they do not distinguish between nucleation and growth. The activation energy of the overall process in bulk materials can be estimated from the present activation energies for nucleation and growth in two dimensions in the following manner: The transformed fraction in an isothermal phase transformation can be conveniently represented by the Johnson-Mehl-Avrami (JMA) model [17,21,22,23] using the following equation

$$\chi(t) = 1 - \exp\left(-k_c t^n\right),$$ (3)

where k_c is the rate constant and n is the Avrami exponent. In the Avrami method, the crystallization activation energy is determined from an Arrhenius relationship of the form

$$t_{50\%} = t_0 \exp\left(\frac{E_a}{k_B T}\right),$$ (4)

where $t_{50\%}$ is the time for 50% crystallization and E_a is the activation energy. From Eq. (3), it follows that

$$t_{50\%} = \left(\frac{0.7}{k_c}\right)^{1/n}.$$ (5)

If crystals nucleate continuously at a constant rate I throughout the transformation and the crystals grow as spheres at a constant rate u, the rate constant $k_c = \pi I u^3/3$ and the Avrami exponent $n = 4$ [17]. Equation (5) can then be written as

$$t_{50\%} = \frac{0.9}{I^{1/4} u^{3/4}}.$$ (6)

According to this equation, the activation energy for the overall crystallization process in bulk materials is related to the present activation energies for nucleation and growth by

$$E_a = \frac{1}{4} E_n + \frac{3}{4} E_g.$$ (7)

As shown in Fig. 7, this value ($E_a = 3.77\pm0.07$ eV) is indeed in very good agreement with the literature data.

3.3 Tailoring the microstructure

The results of the kinetics study suggest that the microstructure of the films should be well represented by the Johnson-Mehl model. This model applies to two-dimensional microstructures that are formed when the nucleation and growth rates are constant. According to this model, the

average grain diameter at impingement can be written as a function of the two-dimensional nucleation and growth rates [24,25]

$$\bar{d} = 1.203 \left(\frac{u}{I} \right)^{\frac{1}{3}},$$ (8)

assuming grain boundaries are immobile after impingement. Fig. 8 compares experimental grain sizes and the values calculated from Eq (8) using the nucleation and growth rates determined in Section 3.2. Very good agreement is achieved between experiments and model with only a slight deviation at low crystallization temperatures. This deviation can be attributed to the long incubation times observed at low temperatures. Any grains that nucleate during the incubation time can grow significantly before other grain nucleate, resulting in a larger average grain size. It is evident from the results in Fig. 8, that the microstructure of near-equiatomic NiTi films is readily tailored by manipulating the nucleation and growth rates: the average grain size of an 800 nm NiTi film can be varied from less than 5 μm to as large as 60 μm depending on the precise crystallization temperature. Given an appropriate heat treatment and in-plane film layout, it may even be possible to grow single-crystal films.

4. Conclusion

In conclusion, we have used an approach based on optical microscopy and AFM to measure for the first time the activation energies of the nucleation and the growth processes for the crystallization of amorphous near-equiatomic NiTi thin films. We propose a simple mechanism that suppresses heterogeneous nucleation, allowing grains to grow in a channeling mode. By manipulating the nucleation and growth rates, unprecedented control over the microstructure of the films is possible.

Acknowledgement

TABLES

Table 1. The Arrhenius parameters for the crystallization of amorphous NiTi in the temperature range from 410 to 445°C.
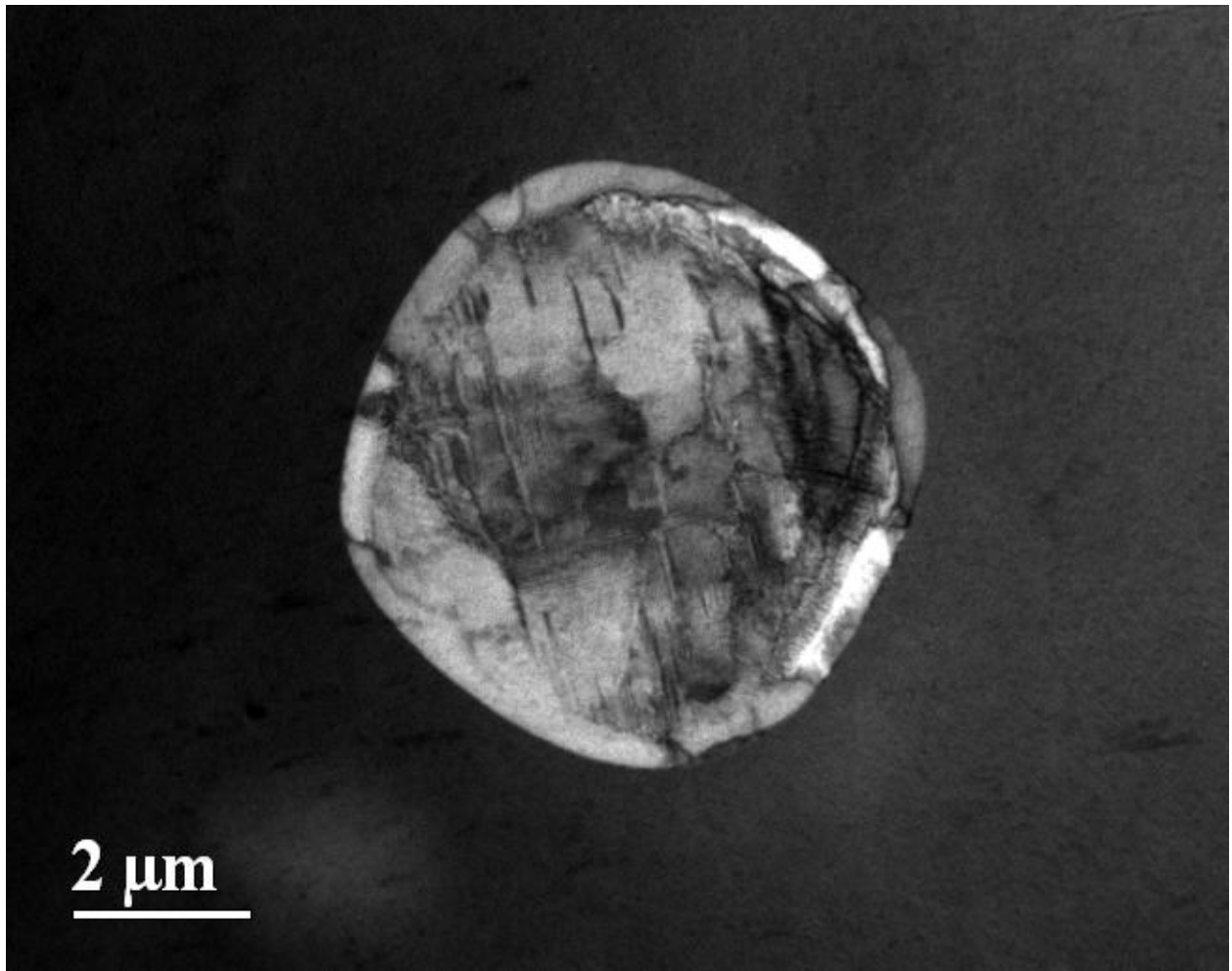
FIGURES

Figure 1. Cross-section TEM of a partially crystallized film.

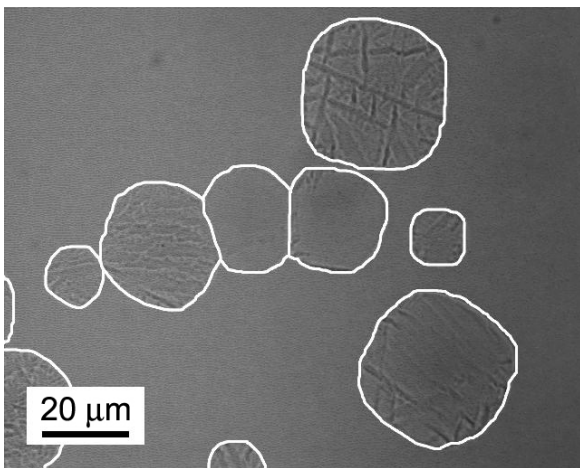Figure 2. Plan-view TEM of a partially crystallized film.

Figure 3. Optical micrographs of a sample subjected to multiple annealing steps (temperature 435 ^{o}C, the times indicated are total time). Crystals have been demarcated with a white line.

Figure 4. Crystal growth velocity as a function of temperature.

Figure 5. Number of nuclei determined from crystal size back-extrapolation (T = 445 ^{o}C), normalized by the untransformed fraction. The nucleation rate is nearly zero during the incubation period and then quickly reaches a steady state value of I_{ss}.

Figure 6. Arrhenius plots of the steady-state nucleation rate and the time lag.

Figure 7. Comparison between the activation energies determined in this work and those in the literature.

Figure 8. Average grain size for an 800nm NiTi film as a function of isothermal annealing temperature. The solid line is calculated from the Johnson-Mehl model.

TABLES

Table 1. The Arrhenius parameters for the crystallization of amorphous NiTi in the temperature range from 410 to 445°C.

Growth velocity u	$\ln(u_0)=47.25\pm0.89$ (u_0 in μms^{-1})	$E_g=3.12\pm0.05$ eV
Nucleation rate I_{ss}	$\ln(I_0)=80.29\pm1.09$ (I_0 in $\mu m^{-3}s^{-1}$)	$E_n=5.72\pm0.14$ eV
Time-lag τ	$\ln(\tau_0)=-44.06\pm5.12$ (τ_0 in s)	$E_\tau=3.03\pm0.31$ eV

FIGURES
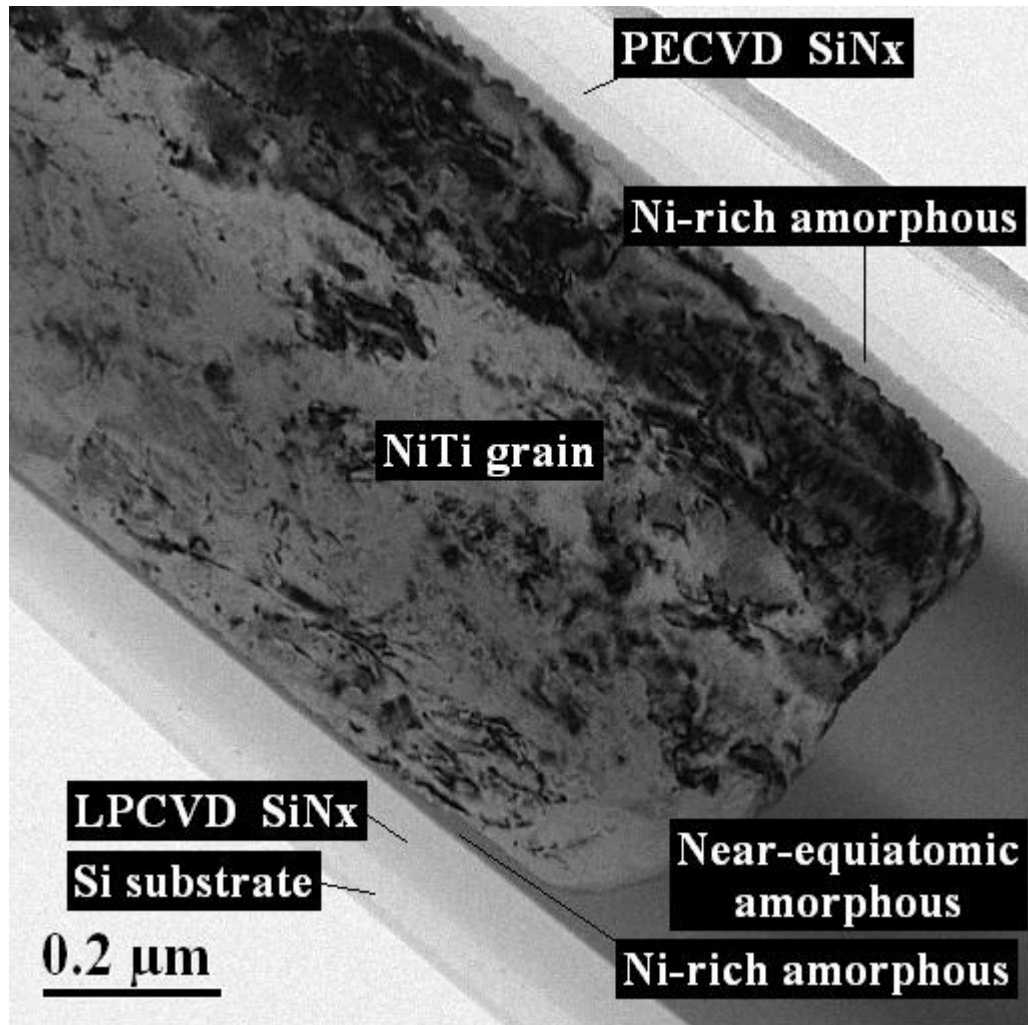
Fig. 1. Cross-section TEM of a partially crystallized film.

Fig. 2. Plan-view TEM of a partially crystallized film.
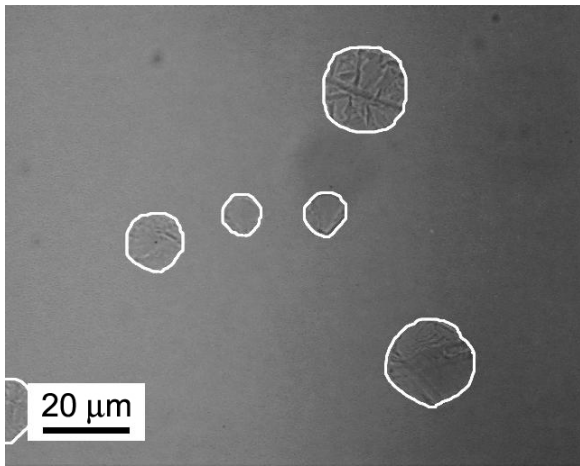
(a) 10 mins
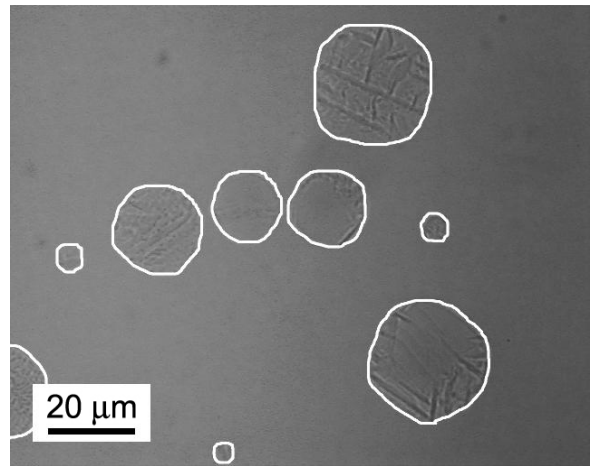
(b) 13 mins

(c) 16 mins
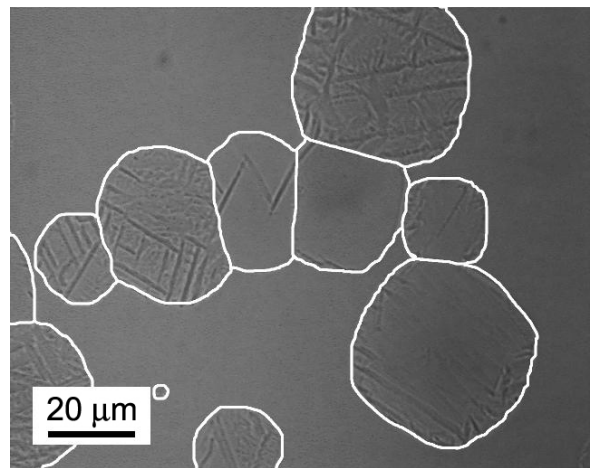
(d) 19 mins

Fig. 3. Optical micrographs of a sample subjected to multiple annealing steps (temperature 435 ^{o}C, the times indicated are total time). Crystals have been demarcated with a white line.
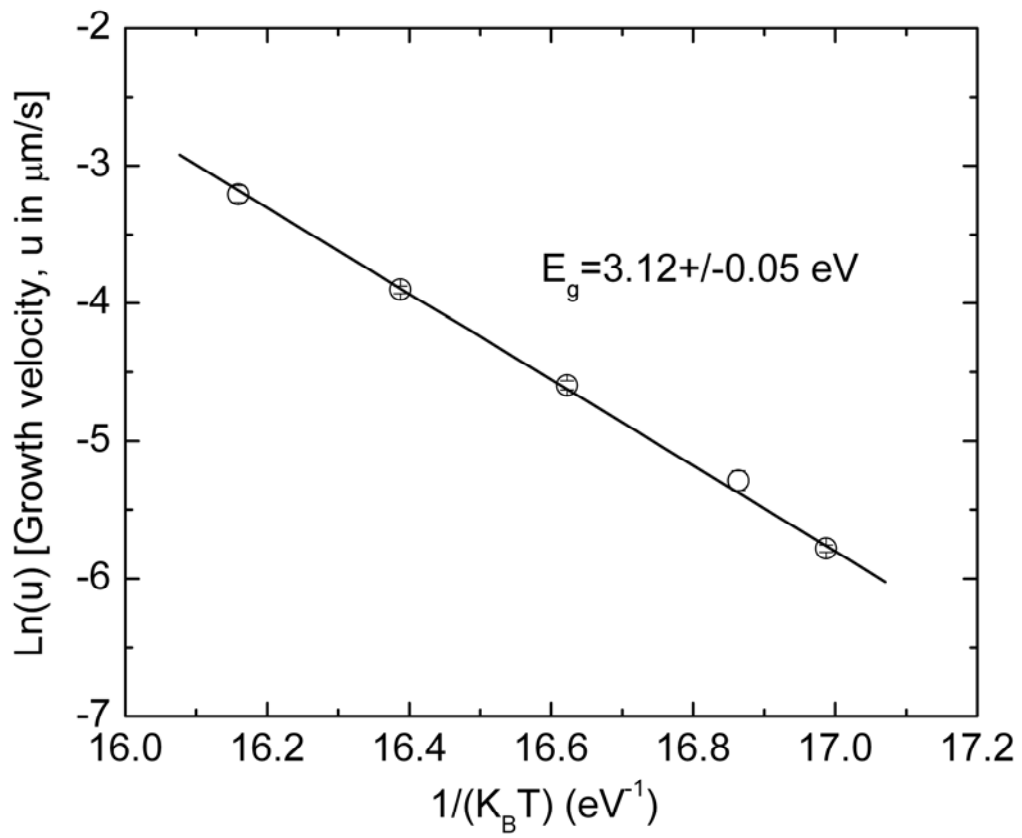
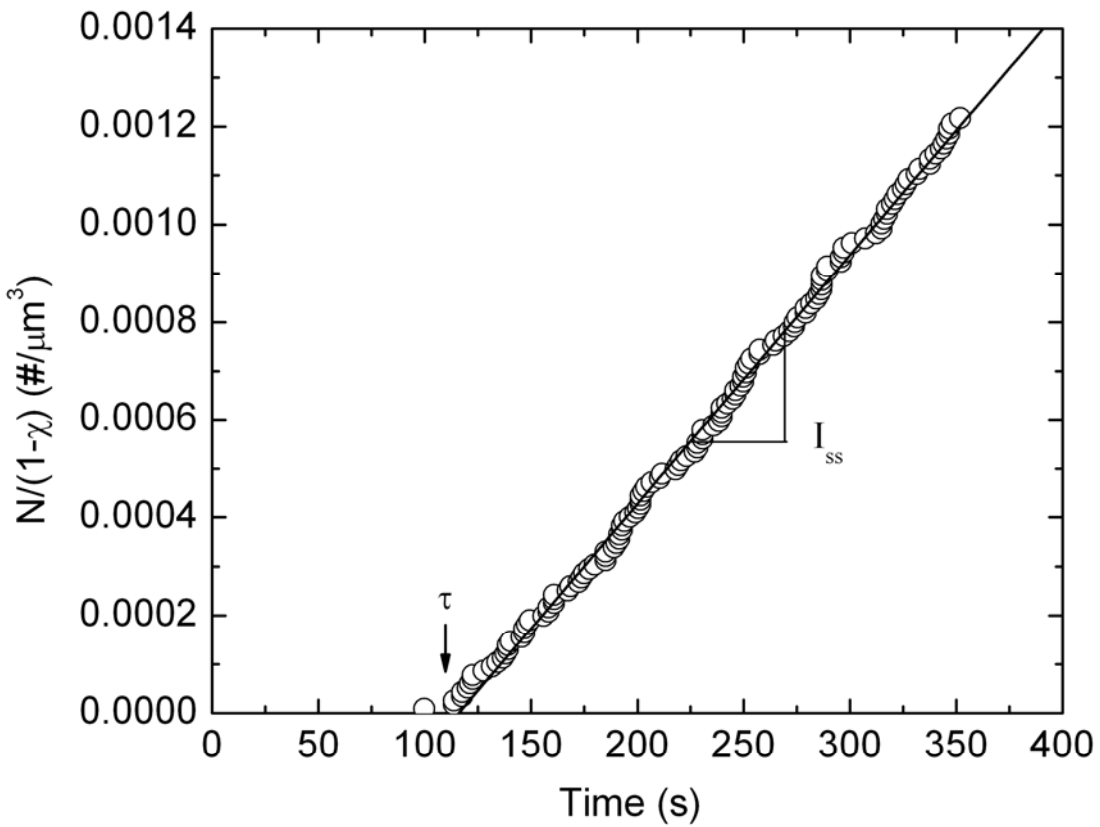Fig. 4. Crystal growth velocity as a function of temperature.

Fig. 5. Number of nuclei determined from crystal size back-extrapolation (T = 445°C), normalized by the untransformed fraction. The nucleation rate is nearly zero during the incubation period and then quickly reaches a steady state value of I_{ss}.
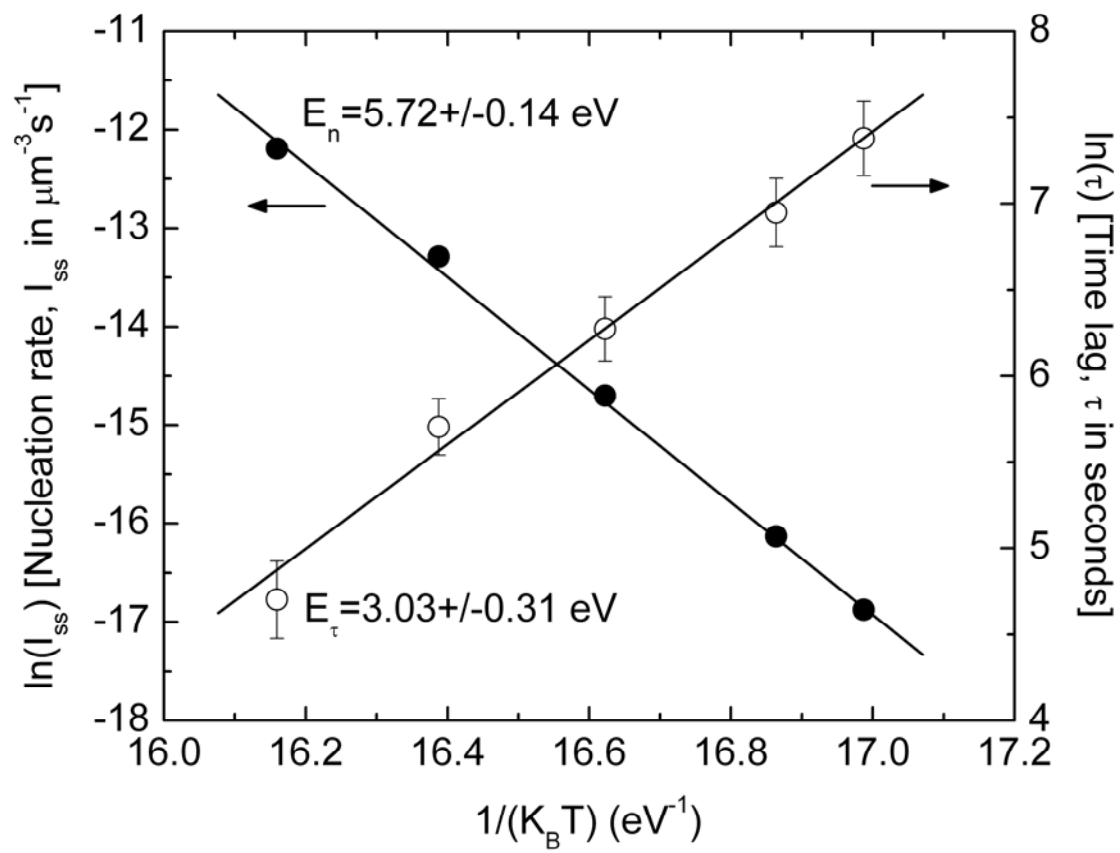
Fig. 6. Arrhenius plots of the steady-state nucleation rate and the time lag.
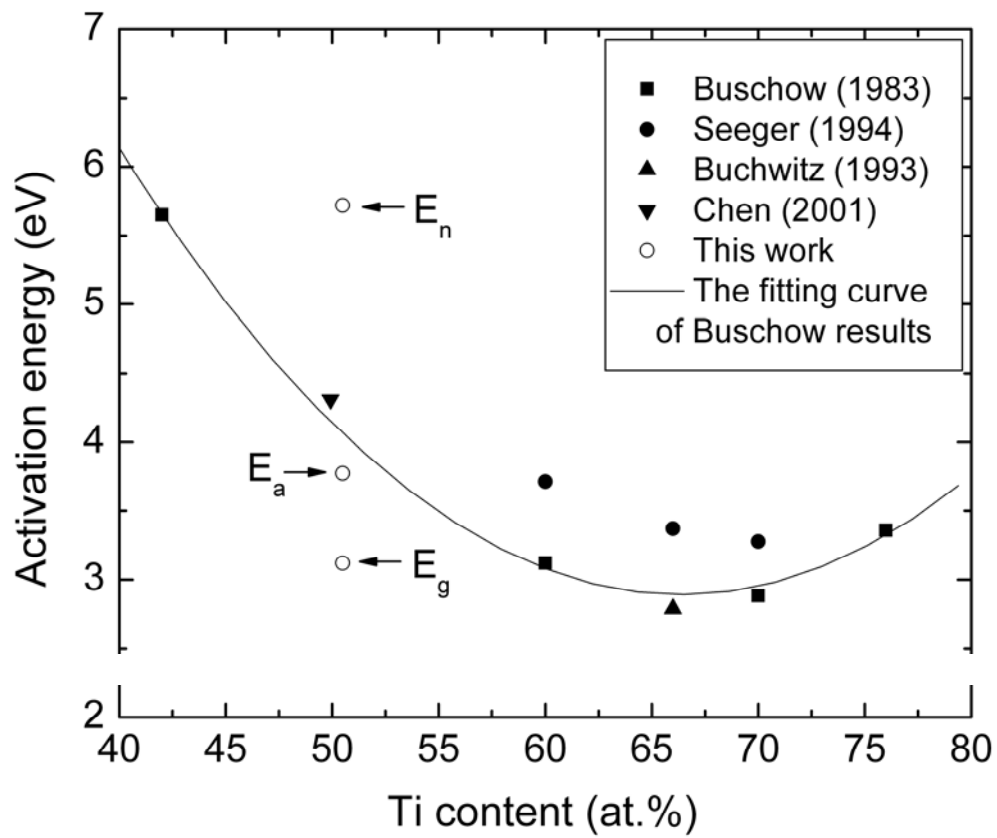
Fig. 7. Comparison between the activation energies determined in this work and those in the literature.
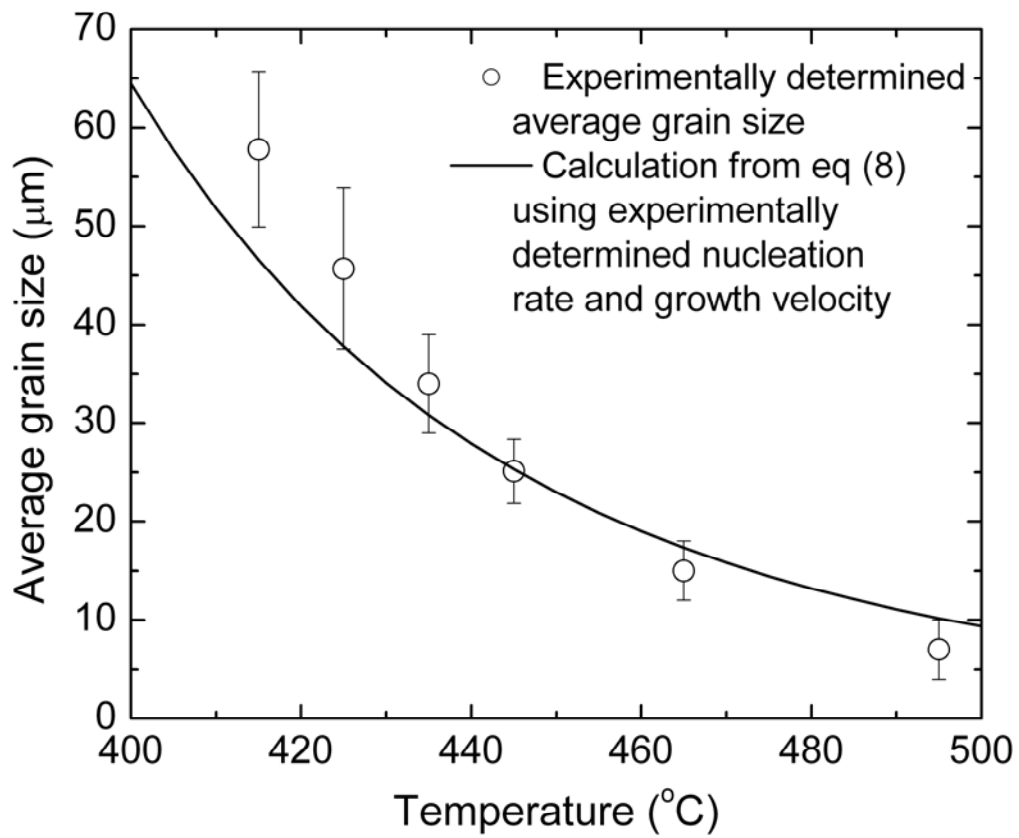
Fig. 8. Average grain size for an 800nm NiTi film as a function of isothermal annealing temperature. The solid line is calculated from the Johnson-Mehl model.

References

[1]   Busch JD, Johnson AD, Lee CH, Stevenson DA. J Appl Phys 1990;68:6224.

[2]   Walker JA, Gabriel KJ, Mehregany M. Sensors and Actuators A 1990;21-23:243.

[3]   Ishida A, Takei A, Miyazaki S. Thin Solid Films 1993;228:210.

[4]   Wolf RH, Heuer AH. J Microelectromech Syst 1995;4:34.

[5]   Miyazaki S, Ishida A. Mater Sci Eng A 1999;273-275:106.

[6]   Grummon DS, Zhang JP. Physica Status Solidi A 2001;186:17.

[7]   Shih CL, Lai BK, Kahn H, Philips SM, Heuer AH. J Microelectromech Syst 2001;10:69.

[8]   Otsuka K, Wayman CM. Shape memory materials. Cambridge: Cambridge University Press, 1998.

[9]   Lehnert T, Crevoiserat S, Gotthardt R. J. Mat. Sci 2002;37:1523.

[10]   Moberly WJ, Busch JD, Johnson AD, Berkson MH. In-situ HVEM crystallization of amorphous TiNi thin films. In: Chen M, Thompson MO, Schwarz RB, Libera M, editors. Phase transformation kinetics in thin films symposium, vol. 230. Anaheim, CA, USA, Materials Research Society; 1991. p. 85-90.

[11]   Lee HJ, Ramirez AG. Appl Phys Lett 2004;85:1146.

[12]   Kalb J, Spaepen F, Wuttig M. Appl Phys Lett 2004;84:5240.

[13]   Kˆster U, Blanke H. Scripta Metall 1983;17:495.

[14]   Buschow KHJ. J Phys F: Met Phys 1983;13:563.

[15]   Chang L, Grummon DS. Phil Mag A 1997;76:163.

[16]   Santamarta R, Schryvers D. Mater Trans A 2003;44:1760.

[17]   Christian JW. The theory of transformation in metals and alloys. 2nd ed. Pergamon, New York, NY, 1975.

[18] Seeger C, Ryder PL. Mater Sci Eng A 1994;179:641.

[19] Buchwitz M, Adlwarth-Dieball R, Ryder PL. Acta Metall Mater 1993;41:1885.

[20] Chen JZ, Wu SK. J Non-Cryst Solids 2001;288:159.

[21] Avrami M. J Chem Phys 1939;7:1103.

[22] Avrami M. J Chem Phys 1940;8:212.

[23] Avrami M. J Chem Phys 1941;9:177.

[24] Tanemura M. Ann Inst Statist Math 1979;31:351.

[25] Frost HJ, Thompson CV. Acta Metall 1987;35:529.